NANO LETTERS

Letter

pubs.acs.org/NanoLett

High-Resolution Distance Dependence Study of Surface-Enhanced Raman Scattering Enabled by Atomic Layer Deposition

Sicelo S. Masango,[†,‡] Ryan A. Hackler,[†,‡] Nicolas Large,[†] Anne-Isabelle Henry,[†] Michael O. McAnally,[†] George C. Schatz,[*,†] Peter C. Stair,[*,†,‡] and Richard P. Van Duyne[*,†]

[†]Department of Chemistry and [‡]Center for Catalysis and Surface Science, Northwestern University, Evanston, Illinois 60208, United States

Supporting Information

ABSTRACT: We present a high-resolution distance dependence study of surface-enhanced Raman scattering (SERS) enabled by atomic layer deposition (ALD) at 55 and 100 °C. ALD is used to deposit monolayers of Al_2O_3 on bare silver film over nanospheres (AgFONs) and AgFONs functionalized with self-assembled monolayers. *Operando* SERS is used to measure the intensities of the Al−CH_3 and C−H stretches from trimethylaluminum (TMA) as a function of distance from the AgFON surface. This study clearly demonstrates that SERS on AgFON substrates displays both a short- and long-range nanometer scale distance dependence. Excellent agreement is obtained between these experiments and theory that incorporates both short-range and long-range terms. This is a high-resolution *operando* SERS distance dependence study performed in one integrated experiment using ALD Al_2O_3 as the spacer layer and Raman label simultaneously. The long-range SERS distance dependence should make it possible to detect chemisorbed surface species located as far as ∼3 nm from the AgFON substrate and will provide new insight into the surface chemistry of ALD and catalytic reactions.

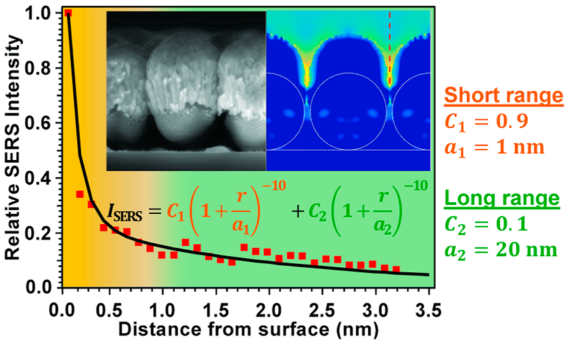

KEYWORDS: *Surface-enhanced Raman scattering, operando, distance dependence, atomic layer deposition*

Surface-enhanced Raman spectroscopy (SERS) is a highly sensitive vibrational spectroscopy technique in which the Raman scattering intensity of molecules close to the surface of a noble metal nanoparticle is amplified by 6−8 orders of magnitude.[1−4] Signal enhancement in SERS is attributed mainly to the electromagnetic (EM) enhancement mechanism.[4,5] The chemical (CHEM) enhancement mechanism is a short-range effect that requires the adsorbate to be chemisorbed directly on the metallic surface and contributes a factor of ∼10 to the total signal enhancement.[6,7] However, the EM enhancement mechanism is a longer-range effect, with a maximum contribution of ∼10^6−10^7. The latter is made possible by excitation of the localized surface plasmon resonance (LSPR) of a noble metal nanoparticle or a nanostructured surface such as Au, Ag, or Cu.[8,9] This results in amplification of the local electromagnetic field around the metal nanostructure, thus leading to more intense scattering of light by molecules in the vicinity of the noble metal nanostructures.

The EM mechanism does not require the analyte of interest to be in direct contact with the metallic surface, but does require it to be within a few nanometers.[4,10] For practical applications such as molecular detection, sensing, and *operando* monitoring of catalytic reactions, it is crucial to determine precisely how the SERS intensity varies with distance from the enhancing surface. Several research groups have investigated the distance dependence of SERS. For example, Kovacs et al. used Langmuir−Blodgett (LB) films of arachidic acid as spacer layers for phthalocyanine molecules on Ag island films to conclude that SERS was due to the EM enhancement mechanism and not from the short-range CHEM enhancement mechanism.[11] Ye et al. investigated the distance dependence of SERS on Ag island films using azobenzene molecules that were covalently linked to an alkanethiol self-assembled monolayer (SAM) whose chain length could be varied from 1 to 15 methylene units. They concluded that the CHEM enhancement mechanism was not the dominant mechanism even at the shortest estimated spacer distances used in their work (∼0.8 nm).[12] Compagnini et al. investigated SERS distance dependence of alkanethiol SAMs by measuring SERS signals coming from just the terminal methyl functional groups and concluded that the SERS distance dependence was due to the EM enhancement mechanism.[13] Limitations of the SERS distance dependence studies published so far include the difficulty associated with controlling the SAM thickness down to a few Ångstroms above the surface. This makes it difficult to investigate short-range contributions to the SERS distance dependence. The orientation of SAMs on rough metallic

Received: March 25, 2016
Revised: May 18, 2016
Published: May 31, 2016

DOI: 10.1021/acs.nanolett.6b01276
Nano Lett. 2016, 16, 4251−4259

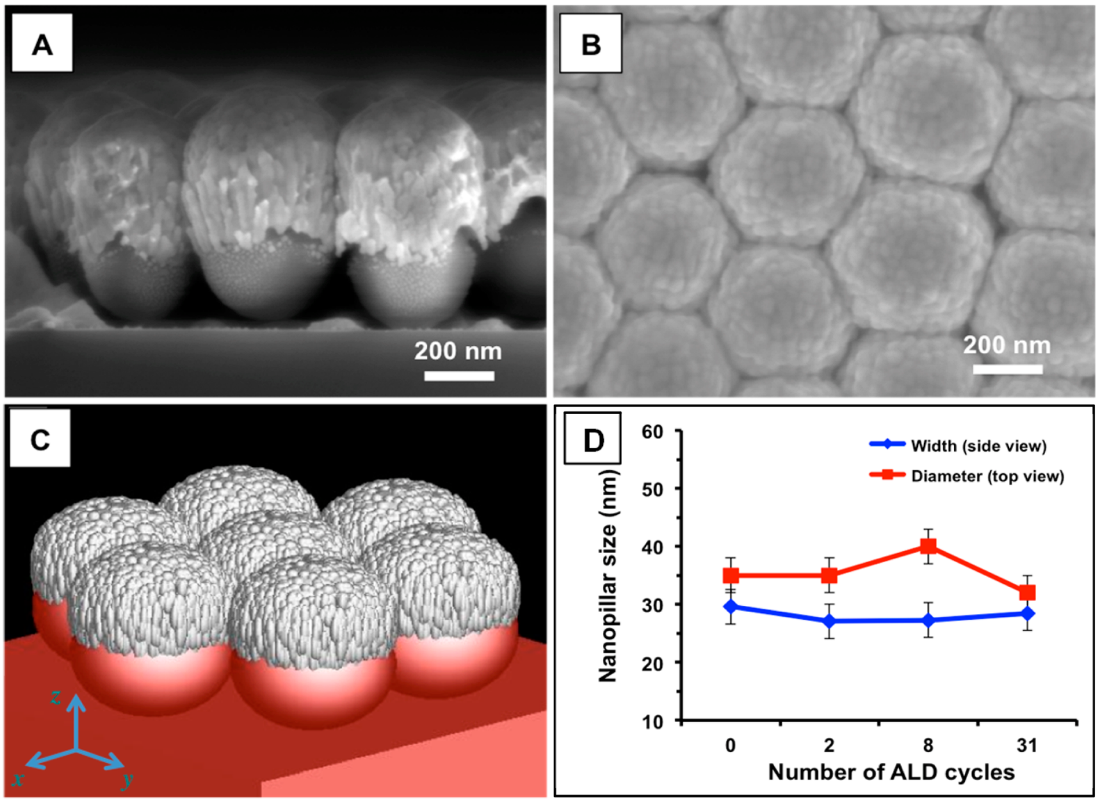

Figure 1. SERS substrate characterization: SEM images of the AgFON substrate from side (A) and top-down (B) observations; the structural features observed experimentally are used in the FDTD-modeled geometry (C) to model the electromagnetic fields at the surface of a realistic AgFON surface. The widths of the nanopillars, i.e., the length of the short axis in the side view (panel A) and the diameter of the spheroidal features in the top-down view (panel B), are reported prior and after ALD coating (D). The error bars in panel D were obtained by estimating to ±3 nm based on the resolution of the SEM images and the precision of the SEM measurements.

nanostructures is also not very well specified, and this can lead to inaccurate values of reported SAM thicknesses. In addition, there is the possibility that defects might be present for poorly formed SAMs, and this makes it challenging to obtain accurate, consistent, and reproducible SERS distance dependence data.[14] Additionally, most previous studies use only a few data points to investigate the SERS distance dependence. For example, Ye et al. used six distance values in their work.[12] More data points are needed in order to capture the full profile of the SERS distance dependence.

The ideal SERS distance dependence experiment would be designed in such a way that the thickness of the spacer could be easily varied in the range from a few Ångstroms to a hundred nanometers. Furthermore, the spacers would be conformal to handle rough nanostructured surfaces, pinhole-free, and chemically uniform. Atomic layer deposition (ALD) is a spacer fabrication method that addresses these challenges and concerns by producing highly uniform films whose thickness can be controlled with Ångstrom-level precision.[15,16] The growth rate of ALD Al_2O_3 is typically ~1.1 Å per cycle.[17] Van Duyne and co-workers previously used ALD Al_2O_3 layers deposited over silver film over nanosphere (AgFON) substrates and investigated the distance dependence of SERS using pyridine as the Raman label.[10] This study concluded that SERS was a long-range effect and good agreement was obtained between experiment and theoretical predictions. Although good agreement was obtained, too few data points were used in that study to rigorously define the distance dependence of SERS. Moreover, the SERS distance dependence experiment was performed *ex situ*, and more than one AgFON substrate had to be used, which increases the uncertainty of the data by averaging results over different substrates.

In the study presented here, the distance dependence of SERS is investigated in one integrated *operando* experiment by using ALD Al_2O_3 as both the spacer layer and Raman label. In addition, our study provides a complete set of data points at ~1 Å resolution both below and above ~1−3 nm for each experimental run. This high spatial resolution is achieved with ALD, which provides thickness control of the deposited Al_2O_3 layer down to the subnanometer level. For applications such as heterogeneous catalysis, ALD Al_2O_3 layers protect SERS substrates against sintering when exposed to high temperatures thus allowing for *operando* monitoring of reactions.[18] The combination of ALD and *operando* SERS allows for investigation of both the short- and long-range distance dependence of SERS using the same substrate. ALD Al_2O_3 spacer layers were also deposited on AgFONs functionalized with benzenethiol and toluenethiol SAMs allowing for SAM peaks to be used as internal standards for spot-to-spot variation in the SERS signal measured across the AgFON surface. Additionally, theoretical methods including electrodynamic calculations using the finite-difference time-domain (FDTD) method and density functional theory (DFT) modeling of surface-bound Raman scattering have been performed to support the experimental findings.

AgFON Structural Characterization and Stability. The AgFON is a robust and optically tunable surface that provides consistent and high electromagnetic enhancement (~10^7) over

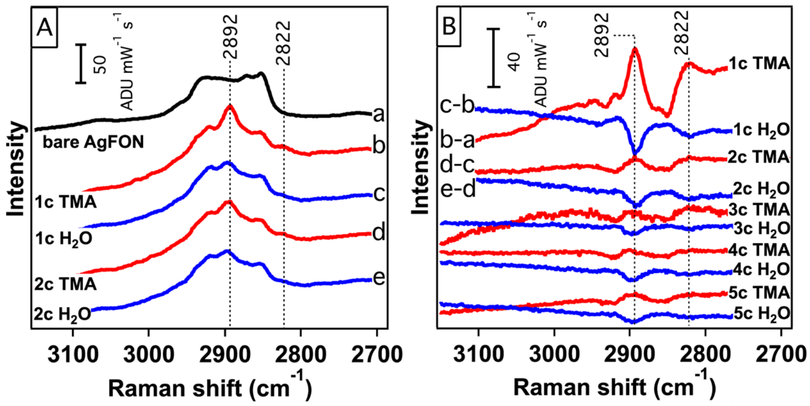

Figure 2. (A) SER spectra of a 25 s Ar plasma-cleaned AgFON before ALD (a) and after 30 s of trimethylaluminum (TMA) (1st cycle; b), 60 s of H_2O (1st cycle; c), 30 s of TMA (2nd cycle; d), and 60 s of H_2O (2nd cycle; e) at 55 °C. (B) Difference SER spectra for the first five ALD Al_2O_3 cycles. SER spectra were acquired with λ_{exc} = 532 nm, P_{exc} = 5 mW, t_{aq} = 10 s, and 10 accumulations each. Data are shifted on the vertical axis for clarity.

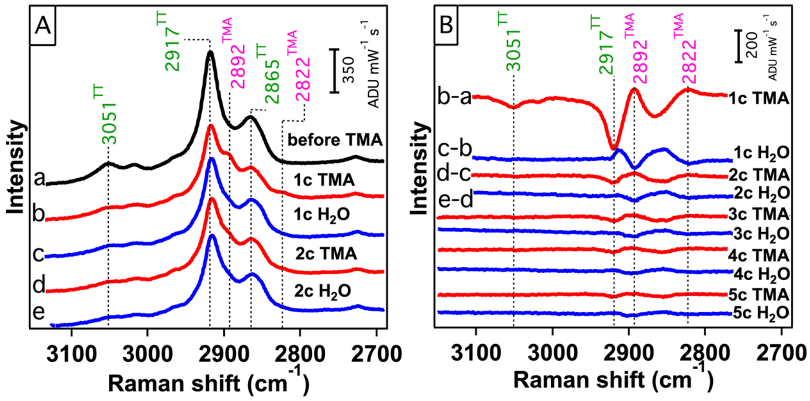

Figure 3. (A) SER spectra of a toluenethiol-functionalized AgFON before ALD (a) and after 10 min of TMA (1st cycle; b), 60 s of H_2O (1st cycle; c), 10 min of TMA (2nd cycle; d), and 60 s of H_2O (2nd cycle, e) at 55 °C. The labels TT and TMA stand for toluenethiol and TMA, respectively. (B) Difference SER spectra for the first two and five ALD cycles. SER spectra were acquired with λ_{ex} = 532 nm, P_{ex} = 1 mW, t_{aq} = 10 s, and 10 accumulations.

large areas (>1 cm^2).[19] Such high enhancement factors (EFs) are comparable to the $\sim 10^6$–10^7 average EFs reported by Wang et al. and Gopinath et al. for extended two-dimensional assemblies.[20,21] It has been shown in a previous study[19] that the functionality of this SERS substrate is strongly correlated to the presence of nanopillars on the surface. Therefore, it is important to infer structure–function relationships in this study. To begin with, we ensured the structural integrity of the AgFON substrate by scanning electron microscopy (SEM, Figure 1). Figure 1A provides a side view observation of the substrate before any ALD. The presence and size of the nanopillars is consistent with previous observations.[19] Figure 1B provides a top-down view of the substrate, showing that the protrusions from the pillars are not solely located on the periphery of the underlying microspheres, but on the whole surface of the film. As we aim to provide a unified view of the electromagnetic properties of the nanostructured metal film, we have used these experimentally measured structural motifs as input parameters for constructing a realistic model geometry for FDTD calculations, as shown in Figure 1C. As the ALD occurs at 55 °C and the thickness of the deposited Al_2O_3 film increases, we might reasonably expect restructuring of the AgFON to occur caused by sintering between adjacent nanopillars. To probe the thermal and structural stability of the AgFONs, we conducted a serial SEM examination of AgFONs, both in side- and top-down views, after 2, 8, and 31 ALD cycles (Figure S3, Supporting Information). From these observations, we demonstrated that sintering of the film does not occur and confirmed the presence of nanopillars throughout the ALD process. We measured and compared the width of 35–90 nanopillars before and after ALD, as plotted in Figure 1D. From this graph, it appears that, statistically, the diameters of the spheroidal caps of the nanopillars (red points and trace) are constant throughout the ALD process. The widths of the nanopillars (blue points and trace) also stay constant with increasing number of ALD cycles. This observation is consistent with a homogeneous growth of the Al_2O_3 film on the entirety of the Ag nanostructured surface, i.e., on both the top and sides of the nanopillars.

C–H Stretches of TMA on Bare AgFON. Figure 2A,B shows SER spectra of a 25 s Ar plasma-cleaned AgFON before and after sequential exposures of TMA and H_2O at 55 °C. Two peaks located at 2892 and 2822 cm^{-1} are observed after TMA exposure and are assigned to two different symmetric C–H stretches of TMA.[22–26] After TMA exposure, the peaks are positive in the SERS difference spectra displayed in Figure 2B and become negative after H_2O exposure. This is because H_2O reacts with the $-(CH_3)_x$ groups on the surface and replaces them with $-(OH)_x$ groups as expected in an Al_2O_3 ALD

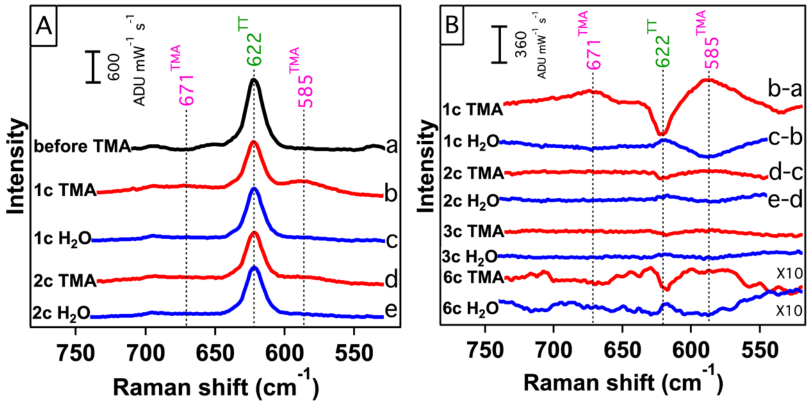

Figure 4. (A) SER spectra of a toluenethiol-functionalized AgFON before ALD (a) and after 10 min of TMA (1st cycle; b), 60 s of H_2O (1st cycle; c), 10 min of TMA (2nd cycle; d), and 60 s of H_2O (2nd cycle; e) at 55 °C. (B) Difference SER spectra for the first two and six ALD Al_2O_3 cycles. SER spectra were acquired with λ_{ex} = 532 nm, P_{ex} = 1 mW, t_{aq} = 2 s, and 10 accumulations.

process. The peaks reappear after TMA exposure because TMA reacts with the $-(OH)_x$ groups and replaces them with $-(CH_3)_x$ groups. The SERS signal decreases as more ALD Al_2O_3 layers are deposited as expected with the distance dependence of the electromagnetic enhancement in SERS (Figure 2B). SER spectra for more than 20 ALD cycles are reported in Figure S4 in the Supporting Information. SERS signals of TMA C−H stretches can be seen even after 25 ALD cycles although they are much weaker (∼10% of the initial intensity).

C−H Stretches of TMA on SAM-Functionalized AgFONs. Figure 3A,B shows SER spectra of a AgFON functionalized with a toluenethiol (TT) SAM before and after ALD Al_2O_3 growth at 55 °C. Two peaks positioned at 2822 and 2892 cm^{-1} are observed after 10 min of TMA exposure. These peaks correspond to two symmetric C−H stretches from TMA.[22,23] The toluenethiol peaks at 2865, 2917, and 3051 cm^{-1} are assigned to the symmetric C−H stretch ($-CH_3$ group), asymmetric C−H stretch ($-CH_3$ group), and the C−H stretch of the phenyl ring, respectively.[27] Since toluenethiol has no reactive sites for TMA, TMA grows directly on the AgFON surface. The decrease in toluenethiol SERS signal after TMA exposure could be due to the displacement of toluenethiol molecules by TMA and orientation changes of toluenethiol molecules on the AgFON.[28] The TMA peaks decay after H_2O exposure and reappear after TMA exposure in the second cycle because of the replacement of $-(CH_3)_x$ and $-(OH)_x$ groups with $-(OH)_x$ and $-(CH_3)_x$ groups, respectively.

As can be seen from the SER difference spectra (Figure 3B), the SERS intensity of the TMA C−H stretches decreases to ∼20% of the initial intensity after the first five ALD Al_2O_3 cycles. Similarly, on a benzenethiol (BT)-functionalized AgFON, C−H stretches appear and decay after TMA and H_2O exposures, respectively, as shown in Figure S5A,B in the Supporting Information. For both toluenethiol- and benzenethiol-functionalized AgFONs, the SERS signals of the TMA C−H stretches can be seen up to at least 10 cycles (∼1 nm away from the surface) and are much weaker in intensity (∼17% of the initial intensity) as displayed in Figure S6A,B in the Supporting Information.

Al−CH_3 Stretches of TMA on SAM-Functionalized AgFONs. Figure 4A,B reports SER spectra of the low frequency region for AgFONs functionalized with a toluenethiol SAM before and after ALD Al_2O_3 growth at 55 °C. Two peaks, assigned to Al−CH_3 stretches of surface-bound TMA species (after TMA exposure), are observed at 585 and 671 cm^{-1}.[28,29] DFT calculations were performed to elucidate the nature of the surface-bound species. The observed Al−CH_3 stretch at 585 cm^{-1} matches closely with the calculated Al−CH_3 asymmetric stretch of dimeric TMA surface species and the Al−CH_3 stretch of monomeric bidentate species as shown in Figure S7B and Table S1 in the Supporting Information. The DFT-modeled dimeric and monomeric molecular structures are shown in Figure S7A in the Supporting Information. The Al−CH_3 stretch at 671 cm^{-1} matches with the calculated symmetric and asymmetric stretch of dimeric and monomeric monodentate surface species, respectively. This mode also matches with the calculated Al−CH_3 stretch of monomeric bidentate species. Based on these results, a variety of dimeric, monodentate, and bidentate TMA species could be present on the AgFON surface. After H_2O exposure, the peaks at 585 and 671 cm^{-1} decay because H_2O reacts with $-(CH_3)_x$ groups of Al$-(CH_3)_x$ surface species and replaces them with $-(OH_3)_x$ groups. The peak at 585 cm^{-1} reappears after TMA exposure because TMA reacts with Al$-(OH)_x$ species and replaces them with Al$-(CH_3)_x$ species. The 671 cm^{-1} peak becomes much weaker after the first ALD cycle. The toluenethiol peak at 622 cm^{-1} is assigned to the combination band of the CCC in-plane bending vibration and C−S stretch.[30,31] Once again, one can see from Figure 4B that the SERS intensity of the Al−CH_3 stretch decreases to ∼12% of the initial intensity after six ALD cycles. The appearance and decay of the Al−CH_3 stretch at 583 cm^{-1} after TMA and H_2O exposures, respectively, on a benzenethiol-functionalized AgFON is shown in Figure S8A,B in the Supporting Information. Similarly, the SERS intensity of the Al−CH_3 stretch decreases to ∼10% of the initial intensity after nine cycles of ALD Al_2O_3 for toluenethiol- and benzenethiol-functionalized AgFONs (Figure S9A,B in the Supporting Information).

High-Resolution SERS Distance Dependence at 55 and 100 °C. Figure 5A shows the high-resolution distance dependence of SERS investigated on AgFONs coated with various thicknesses of ALD Al_2O_3 at 55 °C. The symmetric C−H stretch at 2892 cm^{-1} and symmetric Al−CH_3 stretch at 585 cm^{-1} from TMA were used for analysis. For ALD Al_2O_3 deposited on bare AgFONs, the SERS intensity decreases to ∼20% of the initial intensity when the TMA$-(CH_3)_x$ groups are located at ∼0.7 nm from the surface. Beyond 1 nm the SERS signal decreases less quickly. At a distance of ∼3 nm from

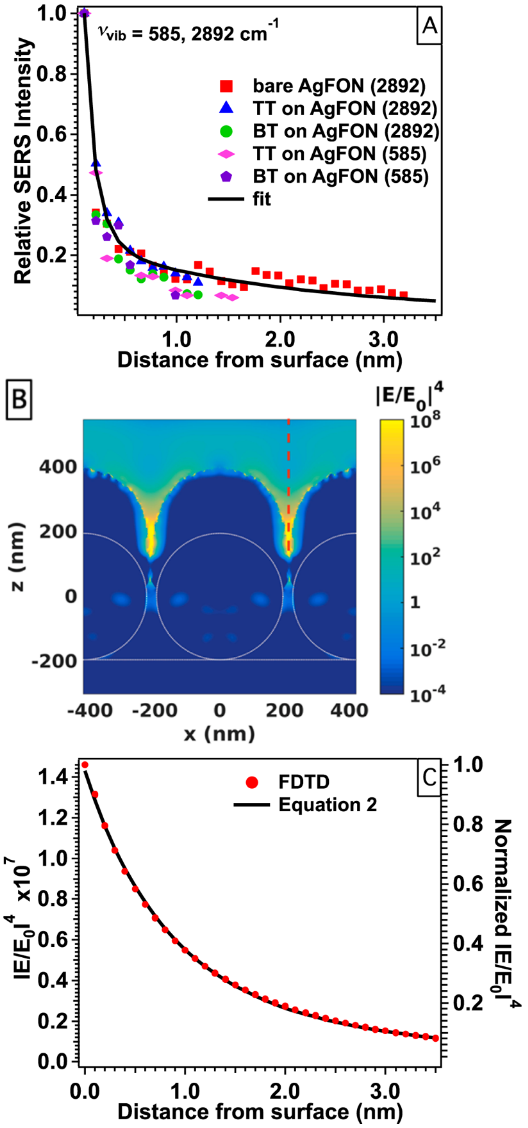

Figure 5. (A) Normalized SERS intensity of the symmetric C−H stretch (from TMA) at 2892 cm^{-1} and symmetric Al−CH$_3$ stretch at 585 cm^{-1} as a function of distance from a bare AgFON and AgFONs functionalized with thiol SAMs. The black solid line is the fit to the data using eq 2. The values of the coefficients C_1 and C_2 extracted from the fit are 0.9 and 0.1, respectively. The radii of curvature a_1 and a_2 are 1 and 20 nm, respectively. The growth rate of Al$_2$O$_3$ was assumed to be 1.1 Å/cycle. Although TMA slightly decreases the intensity of the SAM peaks used for internal calibration (Figure S15), the overall SERS distance dependence trend was similar for bare and functionalized AgFONs. (B,C) FDTD calculations of the near-field distance dependence of a AgFON. Panel B shows the spatial distribution of the fourth power of the local electric field enhancement ($|\mathbf{E}/\mathbf{E}_0|^4$), where $\mathbf{E}_0$ is the incident field. The profiles of the SiO$_2$ spheres and substrate are highlighted with the white dotted lines. Panel C shows the near-field distance dependence at the gap from the metal surface (red dashed line in the cross-section view, panel B). The black solid line is the fit to the FDTD data using eq 2. The normalized values of C_1 and C_2 from the fit are 0.8 and 0.2, respectively. The values of a_1 and a_2 are 8 and 28 nm, respectively.

the surface, the SERS intensity drops to ~7% of the initial SERS signal. A similar trend is observed for ALD Al$_2$O$_3$ deposited on SAM-functionalized AgFONs for both TMA C−H and Al−CH$_3$ stretches. In contrast, Dieringer et al. demonstrated that the SERS intensity decreased to ~60% and ~10% at distances of ~0.7 and ~3 nm for AgFONs, respectively.[10] To account for intensity variations when moving the laser beam from one spot to another on the AgFON surface, the SERS intensity of the TMA Al−CH$_3$ stretch was normalized to the 1080 and 1000 cm^{-1} modes of toluenethiol and benzenethiol SAMs, respectively (Figure S14, Supporting Information). The SERS intensity of the TMA C−H stretch was normalized to the 2917 and 3055 cm^{-1} modes of toluenethiol and benzenethiol SAMs, respectively. Using a simplified sphere model and the $\mathbf{E}^4$ approximation, the distance dependence of SERS is usually represented as

$$I_{\mathrm{SERS}} = \left(1 + \frac{r}{a}\right)^{-10} \tag{1}$$

where I_{SERS} is the SERS intensity of the Raman mode, a is the average dimension of the field enhancing features on the metallic surface (radius of curvature) and r is the distance from the metallic surface to the adsorbate.[32−34] We can clearly see that eq 1 fails to provide a reasonable fit to the experimental data and to capture the full profile of the SERS distance dependence (Figure S10, Supporting Information). To obtain a better fit, it is necessary to account for the short- and long-range SERS effects, by using a two-term phenomenological expression.

$$I_{\mathrm{SERS}} = C_1\left(1 + \frac{r}{a_1}\right)^{-10} + C_2\left(1 + \frac{r}{a_2}\right)^{-10} \tag{2}$$

The parameters a_1, a_2 are the short-range and long-range radii of curvature of AgFON features, respectively, and C_1, C_2 are constants that account for the relative contributions of the two terms. This two-term phenomenological expression is justified by the presence of morphological features of small and large radii of curvature on the AgFON nanostructure as seen in Figure 1A. More generally, most SERS-active substrates can be considered as a heterogeneous collection of roughness features of different sizes and shapes onto which molecules adsorb in a variety of orientations.[35−37] Substrates with varying heterogeneity will have different distance dependence complexities. Molecules adsorbed on the junctions of nanospheres, where the radius of curvature is smaller, experience a different electromagnetic field than molecules adsorbed on surfaces with a large radius of curvature.

Fitting the experimental data to eq 2 leads to a_1 = 1 nm, a_2 = 20 nm, C_1 = 0.9, and C_2 = 0.1. Figure 5B,C shows the near-field distance dependence of a AgFON calculated using FDTD. The cross-section of the near-field distribution (Figure 5B) shows, as expected, a maximum value of $|\mathbf{E}/\mathbf{E}_0|^4$ in the gap between two nanospheres. In some cases, one can also expect strong localized field hotspots at the top of the AgFON, in between pillars and irregularities (Figure S11A, Supporting Information). Figure 5C shows how this local electric field varies when moving away from the metallic surface (red dashed line in panel B). The FDTD calculations clearly show that the field decreases to ~36% and ~10% of the initial intensity at a distance of ~1 and ~3 nm from the surface, respectively. A fit of the FDTD data using eq 2 leads to a_1 = 8 nm, a_2 = 28 nm, C_1 = 0.8, and C_2 = 0.2, in qualitative agreement with the experimental observations in Figure 5A. The observed discrepancy between the experimental and FDTD data at shorter distances (~1 nm) is partially attributed to contributions of the CHEM enhancement mechanism, which are difficult to distinguish from the EM mechanism in the experiment and are not accounted for in the electrodynamic calculations. The CHEM mechanism is expected to play a role beyond just the first ALD cycle until a continuous Al_2O_3 film is formed because it is highly likely that the Al_2O_3 ALD process generates small islands instead of a continuous film during the first few cycles.[38] Additional FDTD calculations of the near-field distance dependence at the gap and top of 570 nm (diameter) AgFONs are provided in Figure S11 in the Supporting Information. In this particular case, where strong plasmonic hotspots are also found at the top of the AgFON, we can see that the near-field decays much quicker (at very short distances of ~1 nm) in the gap region (Figure S11C, Supporting Information) than on the top surface (Figure S11B, Supporting Information) of the AgFONs.

In the present set of experiments, the largest measured distance from the SERS substrate is ~3.2 nm. This distance could be extended by using molecules with larger Raman scattering cross sections than the $Al-(CH_3)_x$ surface species used herein; however, this distance is similar to the longest distances from the SERS substrate typically reported in previous SERS distance dependence studies. For example, Ye et al. reported a long-range SERS distance dependence study using an azobenzene Raman label covalently linked to an alkanethiol SAM for distances of up to ~2.8 nm from the substrate (Ag island film).[12] Similarly, Compagnini et al. measured the SERS distance dependence of the terminal methyl groups of alkanethiol SAMs for distances of up to ~2.5 nm from the substrate (rough Ag foil).[13] Dieringer et al. reported a long-range SERS distance dependence study using pyridine on ALD Al_2O_3 spacer layers for distances up to ~5 nm from the surface of AgFONs.[10] In contrast, Kovacs et al. showed that SERS intensities could be measured at estimated distances of up to ~14 nm from the SERS-active surface.[11] Such large distances are only estimates due to the difficulty in the precise determination of the thickness of the LB films above the Ag island films used. In addition, there is a high probability that defects are present on the surface leaving voids and allowing pthalocyanine molecules to adsorb directly on the Ag island films. This effect could lead to highly enhancing spots with few molecules accounting for the majority of the SERS signal as observed by Dlott et al. leading to erroneous trends at low coverage.[37]

The AgFON surface exhibits nanopillar features,[19] which have small and large radii of curvature (Figure 1). Due to intrinsic measurement limitations, SEM was only able to resolve nanopillar features with large radii of curvature. The value of the a_2 term in eq 2 (20 nm, Figure 5A) is in good agreement with the size of the AgFON nanopillars measured by SEM (~22−40 nm, Figure 1D). During the first few ALD cycles, the SERS signal comes mostly from species adsorbed on the AgFON morphological features with small radii of curvature. FDTD calculations show that the EM field is much higher at the junctions of AgFONs where the radius of curvature is small (Figure 5B). In the modeled geometry (Figure 1C), the gaps narrow down to ~8 nm, in perfect agreement with the 8 nm of the small radius of curvature (a_1) extracted from the fit. This supports the presence of nanometer scale gaps in the actual AgFONs, explaining the very small experimental values of a_1. Subnanometer crevices have also been experimentally evidenced by Wustholz et al. to be correlated with high EM enhancements in a correlated high-resolution transmission electron microscopy-SERS study on single nanoaggregates.[39] As the number of ALD cycles increases, the contribution from the morphological features with large radii of curvature becomes dominant due to the fact that the smaller features are being covered by the Al_2O_3. It can be clearly noticed from Figure 5A that SERS has a short- and long-range distance dependence on AgFON substrates regardless of the vibrational mode investigated. Although, the exact values for C_1, C_2, a_1, and a_2 in eq 2 are expected to change slightly from sample to sample and for the vibrational mode investigated, the overall trend observed in Figure 5A remains highly reproducible. Finally, it can also be inferred from this quantitative description of the EM enhancement profile on AgFON substrates that the density of EM hotspots on this continuous nanostructured metal film is very high. Based on our results, it is clear that the density of EM hotspots is directly correlated to (i) the density of microspheres, via the intersphere crevices, in the short radii of curvature and (ii) the density of nanopillars atop each microsphere in the long radii of curvature dependence. The description of AgFON substrates as “immobilized nanorod assemblies”[19] perfectly encompasses the findings presented herein.

In addition, the distance dependence of SERS was also performed on a 25 s Ar plasma-cleaned AgFON at 100 °C to demonstrate that these substrates could be used to monitor ALD reactions at elevated temperatures. Figure S12A in the Supporting Information depicts the appearance and decay of the symmetric C−H stretches of TMA at 2892 and 2822 cm^{-1} after dosing TMA and H_2O, respectively, at 100 °C. The SERS signals of the TMA C−H stretches were monitored up to 28 ALD cycles and are displayed in Figure S12B in the Supporting Information. Similarly to the experiments performed at 55 °C, the SERS intensity decreases very quickly to ~20% of the initial intensity at a distance of ~1 nm from the surface. The SERS intensity decreases to ~6% at a distance of ~3 nm. Figure S13 in the Supporting Information shows the reduction of the SERS intensity with increasing distance from the surface. Fitting the experimental data using eq 2 resulted in excellent agreement with the two-term phenomenological expression, further supporting the existence of the SERS short- and long-range distance dependence for AgFONs. The scatter in the experimental data for points above and below the fit (solid black line) in Figure S13, Supporting Information, could be explained by SERS intensity variations when changing the laser beam from one spot to another on the AgFON surface. No significant damage to the AgFON was observed during laser irradiation for the laser powers employed in this study as demonstrated in a previous publication.[28] At 55 °C, one might expect to observe ALD growth via condensed TMA. If the Al_2O_3 film were inhomogeneous in thickness due to differences in the amount of condensed TMA across the AgFON, then that could give rise to multiple distance dependences. The fact that the fitting parameters are the same for 55 and 100 °C is significant and points to the lack of condensation contributing to the deposition.

Finally, it is important to notice that, in Figure 5A, the Al_2O_3 film thickness per ALD cycle was consistently assumed to be 1.1 Å for all cycles. However, this estimate is more accurate in later cycles, as the TMA will only interact with hydroxylated Al_2O_3 sites. It remains unknown how far along in our experiment a constant growth rate of 1.1 Å per cycle is reached, if it is not initially at that growth rate. Lu et al. reported that four cycles of Al_2O_3 deposited on both Pd and Pt leads to the formation of Al_2O_3 clusters of 0.4−0.6 nm in height, although their experiment was performed at 200 °C.[40] It is extremely challenging to extract an accurate distance dependence trend at very short distances (≤0.5 nm) because the initial growth rate of Al_2O_3 on a bare AgFON is unknown. Therefore, as a result of the TMA nucleation mechanism and the actual Al_2O_3 initial growth rate, the direct comparison of the experimental and FDTD data at very short distances may be biased by the actual value of the Al_2O_3 thickness after the first few cycles. These two physical effects, which play an important role in the actual experiment, are likely to directly impact the short distance SERS intensity behavior extracted and fitted, thus leading to a deviation from theoretical studies.

In conclusion, we have demonstrated the existence of both short-range and long-range contributions to the distance dependence of SERS. This has been accomplished by using ALD Al_2O_3 as both the spacer layer and Raman label. This work reports the first Ångstrom-resolution *operando* SERS distance dependence study performed in one integrated experiment. On AgFON surfaces, the SERS intensity rapidly drops to ~20% of its initial value at a distance of ~0.7 nm in contrast to what was previously reported. The SERS intensity shows a slower decrease beyond 1 nm from the surface and decreases to ~7% of the initial signal at a distance of ~3 nm. A two-term phenomenological expression that incorporates both short-range and long-range effects, via small and large radii of curvature associated with the morphological features of AgFONs (interspace and diameter of nanopillars), provides an excellent description of the experimentally observed behavior. FDTD calculations of the near-field distance dependence show a quickly and slowly decaying field at a distance of ~1 and ~3 nm from the surface, respectively, strongly supporting the experimental observations. Our results clearly show that SERS has a short- and long-range distance dependence on AgFON substrates. Furthermore, we used the complex effects of TMA nucleation, alumina growth, and chemical enhancement mechanisms, which may also play an important role at very short distances, to rationalize quantitative discrepancies between experiments and calculations. Based on our results, we anticipate that the long-range distance dependence of SERS should enable detection of chemisorbed species located as far as ~3 nm from the AgFON surface during ALD and catalytic reactions. When combined with Fourier transform infrared spectroscopy, the rich molecular structural information provided by *operando* SERS, especially the detection of low frequency metal−oxygen vibrations, will lead to an improved mechanistic understanding of ALD reactions. Further, it is anticipated that *operando* SERS studies of ALD synthesized heterogeneous catalysts will be a very fruitful research area.

Methods. *Fabrication of AgFON SERS Substrates.* AgFONs are ideal SERS substrates as they are relatively simple to fabricate and functionalize while providing relatively homogeneous (±8.6%) high EM enhancement (~10^7) across the substrate.[19,41] AgFONs were fabricated on polished 25 mm silicon wafers according to a standard procedure described in previous published works.[19] Silicon wafers were cleaned by immersion in piranha solution (3:1 by volume H_2SO_4/30% H_2O_2) for 1 h. Clean silicon wafers were thoroughly rinsed with deionized (DI) water. The wafers were then sonicated for 1 h in 5:1:1 by volume H_2O/NH_4OH/30% H_2O_2 followed by rinsing with DI water. Silica nanospheres (390 nm, Bangs Laboratories) were diluted to 5% silica by volume. The solvent was replaced twice with Millipore H_2O (Milli-Q, 18.2 MΩ·cm^{-1}) by a conventional centrifugation/supernatant removal procedure, followed by sonication for 1 h. The solvent-replaced nanosphere solution (10−12 μL) was drop-coated and distributed homogeneously across the silicon wafer surface. The solvent was then allowed to evaporate in ambient conditions and spheres assembled in a hexagonal close-packed array as verified by SEM measurements. Ag films (200 nm) were deposited at a rate of 2 Å/s under vacuum (6×10^{-6} Torr) over the nanospheres using a home-built thermal vapor deposition system. The substrates were spun during deposition, while the metal thickness and deposition rate were measured by a 6 MHz gold-plated QCM (Sigma Instruments, Fort Collins, CO). To remove background carbonaceous contamination, AgFONs were quickly cleaned with reactive ion etching. Plasma cleaning of AgFONs was performed with 392 sccm of Ar in a reactive ion etcher (South Bay Technology, RIE-2000) at 4×10^{-6} Torr and 55 W for 25 s. AgFONs, which were not plasma-cleaned, were incubated in 1 mM ethanolic solutions of benzenethiol and toluenethiol (Sigma-Aldrich) for a minimum of 4 h.

The extinction spectra of AgFONs were measured using a fiber-optic coupled halogen light source (World Precision Instruments) and UV/vis spectrometer (SD 2000, Ocean Optics) in specular reflectance mode with a silver mirror used as a spectral reference. The minimum in reflectance, corresponding to the localized surface plasmon resonance, of a 25 s Ar plasma-cleaned AgFON was optimized for 532 nm laser excitation (cf. reflectance spectrum in Figure S2, Supporting Information).

Scanning electron microscopy (SEM) imaging was performed at the EPIC facility of the NUANCE Center at Northwestern University on a LEO Gemini 1525 microscope (InLens detector) operating at 2−4 kV, with a working distance of 2−4 mm for the side view examination and a working distance of 5−6 mm for the top-down examination.

Surface-Enhanced Raman Spectroscopy. A 532 nm continuous wave (CW) laser (Innovative Photonic Solutions) was used for all the experiments. Laser light was directed, using protected silver mirrors, to a 3 mm right-angle prism and then focused using a visible achromatic doublet lens (1″ diameter, 4″ focal length), through a quartz window to a plasmonic substrate placed inside the ALD reactor. The spot size radius measured at the sample was ~124 μm using a scanning knife-edge technique. Raman scattered light was collected in a 180° backscattering geometry and focused onto a 0.3 m imaging spectrograph (Acton SpectraPro 2300i) using a visible achromatic doublet lens (1″ diameter, 4″ focal length). Scattered light was dispersed by a grating (1200 grooves/mm grating, 500 nm blaze) onto a liquid N_2-cooled CCD detector (Princeton Instruments, Model 7509-0001, 1340 × 400 pixels). SER spectra were collected with 1, 5, or 7 mW of laser power (P_{aq}), 2−10 s of acquisition time (t_{aq}), and 10 accumulations each, depending on the chemical system investigated. No background contribution or SERS signal attenuation was observed from the quartz window. The SERS intensities plotted in Figure 5A were determined from SERS difference spectra by measuring peak heights of the 2892 and 585 cm^{-1} vibrational modes observed after TMA exposure.

Atomic Layer Deposition. ALD was performed in a home-built viscous flow reactor that has been described previously and is shown in Figure S1, Supporting Information.[42,43] SERS substrates were mounted on a movable sample holder, placed inside the ALD chamber under vacuum (~0.05 Torr), and heated to ~55 °C. Another AgFON was cleaned with 25 s of Ar plasma and ALD Al_2O_3 was deposited at 100 °C. SER spectra were acquired before and after dosing 60 sccm of trimethylaluminum (TMA) and 60 sccm H_2O using ultrahigh purity (UHP) N_2 as the carrier gas. The pressure in the reactor was ~1.2 Torr when flowing just 120 sccm of N_2. For one-half-cycle of Al_2O_3, TMA was dosed on bare AgFONs and SAM-functionalized AgFONs for 30 s and 10 min, respectively, and SER spectra were acquired while purging with N_2.[28] The pressure increased from ~1.2 to ~1.4 Torr during TMA exposure. The second half-cycle involved dosing H_2O for 60 s and thereafter acquiring SER spectra during N_2 purging. The pressure increased from ~1.2 to ~1.7 Torr during H_2O exposure. Thermocouples were placed above and below the sample compartment to ensure uniform heating around the sample. Variacs were used to manually adjust the voltage supplied to heating tapes to keep the temperature at 55 or 100 ± 2 °C throughout experiments.

Electrodynamic Calculations. AgFONs were modeled using a random distribution of spherical and spheroidal Ag grains of sizes ranging from 15 to 20 nm dispersed at the upper surface of 390 and 570 nm silica spheres. The silica spheres were placed on a hexagonal lattice where gaps were fixed at 30 nm. The thickness of the Ag film was 200 ± 5 nm. AgFONs were placed on top of a silica substrate, taken as semi-infinite. The FDTD method was used to calculate the near-field properties of AgFONs.[44] The optical source was taken as a linearly polarized broadband plane wave excitation. The FDTD domain was set with proper periodic boundary conditions to mimic an infinitely periodic AgFON. Symmetries were used along the x- and y-directions to minimize the computational cost. Perfectly matched layers (PML) were taken as boundary conditions along the z-direction. A 0.25 nm conformal mesh was used to discretize the rough Ag surface and ensure a good convergence. The rest of the nanostructure was discretized with a 1 nm mesh. An auto-shutoff parameter of 10^{-6} was chosen as a convergence parameter, allowing the fields to propagate for about 10 ns. The dielectric permittivities tabulated by Palik were used for Ag and Si.[45,46]

DFT Calculations. Electronic structure calculations presented in this work have been performed with the Amsterdam Density Functional (ADF) computational chemistry package.[47] Full geometry optimization, frequency, and polarizability calculations for surface bound monomer (both mono- and bidentate) and dimer TMA complexes were completed using the Becke-Perdew (BP86) generalized gradient approximation (GGA) exchange correlation functional and a triple-ζ polarized (TZP) Slater orbital basis set. For the monomer TMA complexes, Ag_{19} and Ag_{20} clusters were used for the surface in monodentate and bidentate binding cases through one or two oxygen atoms, respectively. In the surface bound dimer TMA complex, a Ag_{19} complex was used as a surface, then the dimer TMA was bound to the surface through two oxygen atoms with a bridging methylene group between the aluminum atoms. For more details on molecular structure see Figure S7A in the Supporting Information.

Static Raman polarizabilities ($\omega_{\text{ex}} = 0$) were calculated in the RESPONSE package by two-point numerical differentiation using the RAMANRANGE keyword. Raman scattering intensities were determined by eq 3:[7]

$$\frac{\partial\sigma}{\partial\Omega} = \frac{\pi^2}{\varepsilon_0^2}(\omega - \omega_j)^4 \frac{h}{8\pi c\omega_j}(S)\frac{1}{45\left(1 - \exp\left(-\frac{hc\omega_j}{k_B T}\right)\right)} \qquad (3)$$

where ω is the frequency of the incident laser field, ω_j is the frequency of the jth vibrational mode, and the scattering factor (S) is $45(\overline{\alpha}_j')^2 + 7(\overline{\gamma}_j')^2$; where $\overline{\alpha}_j'$, $\overline{\gamma}_j'$ are the isotropic and anisotropic polarizability tensors with respect to the jth vibrational mode. The Raman intensity for each vibrational mode was broadened to a Lorentzian line shape with full width at half-maximum (fwhm) of 20 cm^{-1} for comparison to experimental data.

ASSOCIATED CONTENT

Supporting Information

The Supporting Information is available free of charge on the ACS Publications website at DOI: 10.1021/acs.nanolett.6b01276.

> Experimental apparatus, extinction spectra of AgFONs, SEM images of AgFONs, SER spectra of more cycles of ALD Al_2O_3 on AgFONs, SERS distance dependence results at 100 °C, FDTD results for a 570 nm AgFON, and DFT calculated Raman spectra of surface-bound species (PDF)

AUTHOR INFORMATION

Corresponding Authors

*E-mail: schatz@chem.northwestern.edu.
*E-mail: pstair@northwestern.edu.
*E-mail: vanduyne@northwestern.edu.

Author Contributions

S.S.M. and R.A.H. carried out the sample fabrication and SERS distance dependence experiments, N.L. performed the FDTD and theoretical analysis, A.-I.H. performed the SEM structural analysis, and M.O.M. performed DFT calculations. All authors discussed and interpreted the results. The manuscript was written through contributions of all authors. All authors have given approval to the final version of the manuscript.

Notes

The authors declare no competing financial interest.

ACKNOWLEDGMENTS

The authors gratefully acknowledge financial support from the Northwestern University Institute for Catalysis in Energy Processes (ICEP). ICEP is funded through the US Department of Energy, Office of Basic Energy Sciences (Award Number DE-FG02-03-ER15457). Funding from the Air Force Office of Scientific Research MURI (FA9550-14-1-0003) is also acknowledged. This material is also based on research sponsored by the Air Force Research Laboratory under agreement FA8650-15-2-5518. The U.S. Government is authorized to reproduce and distribute reprints for Governmental purposes notwithstanding any copyright notation thereon. The views and conclusions contained herein are those of the authors and should not be interpreted as necessarily representing the official policies or endorsements, either expressed or implied, of Air Force Research Laboratory or the U.S. Government. M.O.M. acknowledges support from the National Science Foundation Graduate Fellowship Research Program under Grant No. DGE-0824162. This work made use of the EPIC facility of the NUANCE Center at Northwestern University, which has received support from the Soft and Hybrid Nanotechnology Experimental (SHyNE) Resource (NSF NNCI-1542205); the MRSEC program (NSF DMR-1121262) at the Materials Research Center; the International Institute for Nanotechnology (IIN); the Keck Foundation; and the State of Illinois, through the IIN. Computational resource was provided by the Quest high performance computing facility at Northwestern University, which is jointly supported by the Office of the Provost, the Office for Research, and Northwestern University Information and Technology (NUIT).

REFERENCES

(1) Jeanmaire, D. L.; Van Duyne, R. P. *J. Electroanal. Chem. Interfacial Electrochem.* **1977**, *84*, 1−20.

(2) Dieringer, J. A.; Lettan, R. B.; Scheidt, K. A.; Van Duyne, R. P. *J. Am. Chem. Soc.* **2007**, *129*, 16249−16256.

(3) Zrimsek, A. B.; Henry, A.-I.; Van Duyne, R. P. *J. Phys. Chem. Lett.* **2013**, *4*, 3206−3210.

(4) Stiles, P. L.; Dieringer, J. A.; Shah, N. C.; Van Duyne, R. P. *Annu. Rev. Anal. Chem.* **2008**, *1*, 601−626.

(5) Lombardi, J. R.; Birke, R. L. *J. Phys. Chem. C* **2008**, *112*, 5605−5617.

(6) Campion, A.; Ivanecky, J. E., III; Child, C. M.; Foster, M. *J. Am. Chem. Soc.* **1995**, *117*, 11807−11808.

(7) Valley, N.; Greeneltch, N. G.; Van Duyne, R. P.; Schatz, G. C. *J. Phys. Chem. Lett.* **2013**, *4*, 2599−2604.

(8) Schatz, G. C.; Van Duyne, R. P. In *Handbook of Vibrational Spectroscopy*; Chalmers, J. M., Griffiths, P. R., Eds.; Wiley: New York, 2002; pp 759−774.

(9) Willets, K. A.; Van Duyne, R. P. *Annu. Rev. Phys. Chem.* **2007**, *58*, 267−297.

(10) Dieringer, J. A.; McFarland, A. D.; Shah, N. C.; Stuart, D. A.; Whitney, A. V.; Yonzon, C. R.; Young, M. A.; Zhang, X.; Van Duyne, R. P. *Faraday Discuss.* **2005**, *132*, 9−26.

(11) Kovacs, G. J.; Loutfy, R. O.; Vincett, P. S.; Jennings, C.; Aroca, R. *Langmuir* **1986**, *2*, 689−694.

(12) Ye, Q.; Fang, J.; Sun, L. *J. Phys. Chem. B* **1997**, *101*, 8221−8224.

(13) Compagnini, G.; Galati, C.; Pignataro, S. *Phys. Chem. Chem. Phys.* **1999**, *1*, 2351−2353.

(14) Schoenfisch, M. H.; Pemberton, J. E. *J. Am. Chem. Soc.* **1998**, *120*, 4502−4513.

(15) George, S. M. *Chem. Rev.* **2010**, *110*, 111−131.

(16) Puurunen, R. L. *J. Appl. Phys.* **2005**, *97*, 121301−121352.

(17) Whitney, A. V.; Elam, J. W.; Zou, S.; Zinovev, A. V.; Stair, P. C.; Schatz, G. C.; Van Duyne, R. P. *J. Phys. Chem. B* **2005**, *109*, 20522−20528.

(18) Whitney, A. V.; Elam, J. W.; Stair, P. C.; Van Duyne, R. P. *J. Phys. Chem. C* **2007**, *111*, 16827−16832.

(19) Greeneltch, N. G.; Blaber, M. G.; Henry, A.-I.; Schatz, G. C.; Van Duyne, R. P. *Anal. Chem.* **2013**, *85*, 2297−2303.

(20) Wang, D.; Zhu, W.; Best, M. D.; Camden, J. P.; Crozier, K. B. *Sci. Rep.* **2013**, *3*, 2867.

(21) Gopinath, A.; Boriskina, S. V.; Reinhard, B. M.; Dal Negro, L. *Opt. Express* **2009**, *17*, 3741−3753.

(22) Ferguson, J. D.; Weimer, A. W.; George, S. M. *Chem. Mater.* **2004**, *16*, 5602−5609.

(23) Soto, C.; Tysoe, W. T. *J. Vac. Sci. Technol., A* **1991**, *9*, 2686−2695.

(24) George, S. M.; Ott, A. W.; Klaus, J. W. *J. Phys. Chem.* **1996**, *100*, 13121−13131.

(25) Goldstein, D. N.; McCormick, J. A.; George, S. M. *J. Phys. Chem. C* **2008**, *112*, 19530−19539.

(26) Sano, H.; Mizutani, G.; Ushioda, S. *Chem. Phys. Lett.* **1992**, *194*, 398−402.

(27) Sebek, J.; Knaanie, R.; Albee, B.; Potma, E. O.; Gerber, R. B. *J. Phys. Chem. A* **2013**, *117*, 7442−7452.

(28) Masango, S. S.; Hackler, R. A.; Henry, A.-I.; McAnally, M. O.; Schatz, G. C.; Stair, P. C.; Van Duyne, R. P. *J. Phys. Chem. C* **2016**, *120*, 3822−3833.

(29) Ogawa, T. *Spectrochim. Acta* **1968**, *24A*, 15−20.

(30) Joo, T. H.; Kim, M. S.; Kim, K. *J. Raman Spectrosc.* **1987**, *18*, 57−60.

(31) Lee, T. G.; Kim, K.; Kim, M. S. *J. Raman Spectrosc.* **1991**, *22*, 339−344.

(32) Kennedy, B. J.; Spaeth, S.; Dickey, M.; Carron, K. T. *J. Phys. Chem. B* **1999**, *103*, 3640−3646.

(33) Murray, C. A. In *Surface Enhanced Raman Scattering*; Chang, R. K., Furtak, T. E., Eds.; Plenum: New York, 1982; pp 203−221.

(34) Pettinger, B.; Domke, K. F.; Zhang, D.; Picardi, G.; Schuster, R. *Surf. Sci.* **2009**, *603*, 1335−1341.

(35) Campion, A.; Kambhampati, P. *Chem. Soc. Rev.* **1998**, *27*, 241−250.

(36) Zhang, Q.; Large, N.; Nordlander, P.; Wang, H. *J. Phys. Chem. Lett.* **2014**, *5*, 370−374.

(37) Fang, Y.; Seong, N.-H.; Dlott, D. D. *Science* **2008**, *321*, 388−392.

(38) Lu, J.; Liu, B.; Greeley, J. P.; Feng, Z.; Libera, J. A.; Lei, Y.; Bedzyk, M. J.; Stair, P. C.; Elam, J. W. *Chem. Mater.* **2012**, *24*, 2047−2055.

(39) Wustholz, K. L.; Henry, A.-I.; McMahon, J. M.; Freeman, R. G.; Valley, N.; Piotti, M. E.; Natan, M. J.; Schatz, G. C.; Van Duyne, R. P. *J. Am. Chem. Soc.* **2010**, *132*, 10903−10910.

(40) Lu, J.; Liu, B.; Guisinger, N. P.; Stair, P. C.; Greeley, J. P.; Elam, J. W. *Chem. Mater.* **2014**, *26*, 6752−6761.

(41) Greeneltch, N. G.; Blaber, M. G.; Schatz, G. C.; Van Duyne, R. P. *J. Phys. Chem. C* **2013**, *117*, 2554−2558.

(42) Masango, S. S.; Peng, L.; Marks, L. D.; Van Duyne, R. P.; Stair, P. C. *J. Phys. Chem. C* **2014**, *118*, 17655−17661.

(43) Elam, J. W.; Groner, M. D.; George, S. M. *Rev. Sci. Instrum.* **2002**, *73*, 2981−2987.

(44) Lumerical Solutions, Inc. FDTD Solutions. http://lumerical.com/tcad-products/fdtd/ (accessed 04/24/2016).

(45) Lynch, D. W.; Hunter, W. R. In *Handbook of Optical Constants of Solids*; Palik, E. D., Ed.; Academic Press: Burlington, MA, 1997; Vol. *1*, pp 275−367.

(46) Edwards, D. F. In *Handbook of Optical Constants of Solids*; Palik, E. D., Ed.; Academic Press: Burlington, MA, 1997; Vol. *1*, pp 547−569.

(47) Baerends, E. J.; Ziegler, T.; Autschbach, J.; Bashford, D.; Berces, A.; Bickelhaupt, F. M.; Bo, C.; Boerrigter, P. M.; Cavallo, L.; Chong, D. P.; et al. *ADF2014*; SCM, Theoretical Chemistry, Vrije Universiteit: Amsterdam, The Netherlands; http://www.scm.com.